Published in : ChemSusChem (2022), vol. 15, n°18, e202200913
DOI: doi.org/10.1002/cssc.202200913
Status : Postprint (Author's version)

BIO-BASED SOLID ELECTROLYTES BEARING CYCLIC CARBONATES FOR SOLID-STATE LITHIUM METAL BATTERIES

Ashish Raj,[a] Satyannarayana Panchireddy,[a] Bruno Grignard,[b] Christophe Detrembleur,[b] and Jean-François Gohy[a]

[a] A. Raj, Dr. S. Panchireddy, Prof. J.-F. Gohy
Institute of Condensed Matter and Nanoscience (IMCN)
Université catholique de Louvain
Place L. Pasteur 1, 1348 Louvain-la-Neuve (Belgium)
E-mail: jean-francois.gohy@uclouvain.be

[b] Dr. B. Grignard, Dr. C. Detrembleur
Center for Education and Research on Macromolecules (CERM),
CESAM Research Unit, University of Liège
Allée du 6 août, Building B6A, 4000 Liège (Belgium)

KEYWORDS : electrochemistry; electrolytes; energy storage; LiTFSI; lithium batteries

ABSTRACT

Green resources for lithium-based batteries excite many researchers due to their eco-friendly nature. In this work, a sustainable bio-based solid-state electrolyte was developed based on carbonated soybean oil (CSBO), obtained by organocatalyzed coupling of CO_2 to epoxidized soybean oil. CSBO coupled with lithium bis(trifluoromethanesulfonyl)imide salt on a bio-based cellulose separator resulted in free-standing membranes. Those membranes on electrochemical measurements exhibited ionic conductivity of around 10^{-3} S cm^{-1} at 100 °C and around 10^{-6} S cm^{-1} at room temperature with wide electrochemical stability window (up to 4.6 V vs. Li/Li$^+$) and transference number up to 0.39 at RT. Further investigations on the galvanostatic charge-discharge of $LiFePO_4$ cathodes with CSBO-based electrolyte membranes and lithium metal anodes delivered the gravimetric capacity of 112 and 157 mAh g^{-1} at RT and 60 °C, respectively, providing a promising direction to further develop bio-based solid electrolytes for sustainable solid-state lithium batteries.

Published in : ChemSusChem (2022), vol. 15, n°18, e202200913
DOI: doi.org/10.1002/cssc.202200913
Status : Postprint (Author's version)

Introduction

Energy storage devices like metal-ion, metal-air, and other classes of batteries have revolutionized our modern life by entering in numerous everyday life and industrial applications ranging from portable electronic devices to electric vehicles and stationary power grids, just to name a few. In this context, lithium-ion batteries have been of much interest for more than three decades owing to their high energy density (250 Wh kg^{-1}) and durability. Until now, the market is dominated by lithium-ion batteries based on conventional liquid electrolytes with lithium ions shuttling between cathodes like $LiFePO_4$ (LFP), $LiCoO_2$ (LCO), and so on, and anodes based on graphite and silicon,[1] although lithium metal-based anodes with their lower potential and higher capacity (3860 mAh g^{-1}) have drawn researchers' interest for a longer time.[2, 3] Lithium metal anodes exposed to liquid electrolytes soaked in separators pose major issues in terms of safety, electrolyte leakage, and dendrites growth, ultimately resulting in short-circuit, intense heating, and flammability.[4-6] Consequently, there is a strong need and increasing market demand for solid-state batteries containing solid electrolytes (SEs) as a potential alternative.[7, 8] SEs can provide not only high energy and power density but may also enhance the safety and durability of batteries.[9] In addition to the design of new solid electrolytes, a large number of studies are also being dedicated to the understanding of the long cycling cells failure via interfacial studies and thus engineering interfaces for beneficial solid electrolyte interphase (SEI) species either by surface treatments and computational predictions.[10-12] For example, self-healing materials and coatings gained focus on preventing physical and chemical damage and achieving sustainability, lower environmental impact over the lifetime, and better acceptability.[13-16]

As lithium-metal batteries are maturing with time, the clock ticks not only on the improvement of existing Li-ion cells but also beyond Li-ion batteries technologies, keeping in mind that the former poses issues like stability, limited Li reserves, and recycling.[17-20] Alternatives like sodium-, potassium-, or magnesium-based batteries, just to name a few, have been actively studied.[21-24] Sustainable materials have also reached momentum for the fabrication of the next generation of batteries. For instance, sustainable gel-polymer/solid-state electrolytes are being developed to overcome the hurdles of safety, stability, and dendrite growth.[25-28] Recently, Bella and co-workers designed lignin-based membranes by crosslinking of a pre-oxidized Kraft lignin matrix with an ethoxylated difunctional oligomer. Those gel polymer electrolytes (GPEs) exhibited decent conductivity of 10^{-3} S cm^{-1} and >4 V stability window with K^+.[29] However, it is still early to compare the market reality of other metal-ion batteries to lithium-based ones due to insufficient understanding of those new technologies. All-solid-state batteries based on lithium are thus still a strong bet for high energy and power density to fulfil immediate future needs toward a clean energy path.[26]

Upon discovery of poly(ethylene oxide) (PEO) as an ion conductor by Wright and co-workers[30] and Armand,[31] PEO-based solid polymer electrolytes (SPEs) received a lot of attention since they allow efficient dissolution and dissociation of lithium salts, ionic transport due to the so-called ion-hopping mechanism, and the typical viscoelastic properties of polymers for the formation of free-

Published in : ChemSusChem (2022), vol. 15, n°18, e202200913
DOI: doi.org/10.1002/cssc.202200913
Status : Postprint (Author's version)

standing membranes. However, PEO-based devices have demonstrated low to moderate performance in the long run due to their low lithium transference number (<0.2) and limited electrochemical stability window (<4 V).[32] Moreover, PEO-based batteries need to operate at temperatures higher than the melting point of PEO (≈60 °C) since lithium ions transport is considerably slowed down in crystalline PEO domains. Research is thus now directed towards developing new SPEs outperforming PEO-based systems.

In recent years, electrolytes based on amorphous polycarbonates mimicking low-molar-mass carbonated liquid electrolytes have emerged as alternatives to PEO due to their lithium ions transport properties, high transference number, good electrochemical stabilities, and tailored mechanical properties. Generally, cyclic carbonates were introduced as side-chains in polymers, while linear carbonates were incorporated in the polymer backbone. As a typical example, Chai et al. polymerized vinylene carbonate to obtain a linear polymer with cyclic carbonate in the polymer backbone.[33] Lex-Balducci and co-workers copolymerized a methacrylate bearing cyclic carbonate side-chains with oligo(ethylene glycol) methacrylate and prepared gel polymer electrolytes by swelling the accordingly obtained copolymers in a carbonate-based electrolyte.[34, 35] We investigated SPEs based on cyclic carbonate trifluoromethacrylate and vinylidene fluoride units[36] and random copolymers of *n*-butylacrylate and cyclic carbonate bearing acrylate.[37] Zhang et al. described a linear poly(propylene carbonate) providing an ionic conductivity of 10^{-4} S cm^{-1} at room temperature.[38] Tominaga and co-workers synthesized linear poly(ethylene carbonate) that was further integrated in a hybrid membrane, reaching an ionic conductivity of 10^{-5} S cm^{-1} at 30 °C.[39, 40] In another study, Tominaga and co-workers combined carbonate and ether units in a copolymer, which was obtained by copolymerization of ethylene oxide with CO_2.[41] Copolymers composed of polyether segments and linear carbonates were reported by Mecerreyes and co-workers.[42] The influence of the incorporation of cyclic carbonates within the chains was also studied by the same group.[43] The quest for environment-friendly electrolytes has motivated researchers to investigate "green" polymers in SPEs.[44] These polymers include poly(lactic acid)[45, 46] and polyurethanes due to their high degree of tuneability in mechanical properties and conductivity as highlighted in recent Reviews and articles.[13, 47-50] In this context, polymers based on vegetable oils with long fatty acids,[51-53] cellulose,[54] gums,[55] and others similar bio-derivatives[56, 57] are of high interest as potential ion conductors owing to their ether and carbonyl functional groups.

Motivated by the urgent need of more sustainable materials for battery applications, we designed a novel bio- and CO_2-based solid electrolyte derived from soybean oils bearing cyclic carbonate units on triglyceride fatty acid segments and CO_2 (as shown in Scheme 1). The cyclic carbonated soybean oil (CSBO) not only confers a sustainable character to the electrolyte for lithium-ion battery, but it is also environmentally safe, easy to process, and easily accessible at the multi-kg scale.[58] In addition, a high density of polar cyclic carbonate units can improve the salt dissolution and reduce the activation energy for ion hopping from one polar group to another.[59] We investigate the influence of the electrolyte system loaded with different amounts of lithium bis(trifluoromethanesulfonyl)imide (LiTFSI), characterized for electrochemical and thermal properties. We also demonstrate the galvanostatic charge-discharge of LFP and lithium metal coin cell with our bio-based CSBO solid electrolyte.

Published in : ChemSusChem (2022), vol. 15, n°18, e202200913
DOI: doi.org/10.1002/cssc.202200913
Status : Postprint (Author's version)

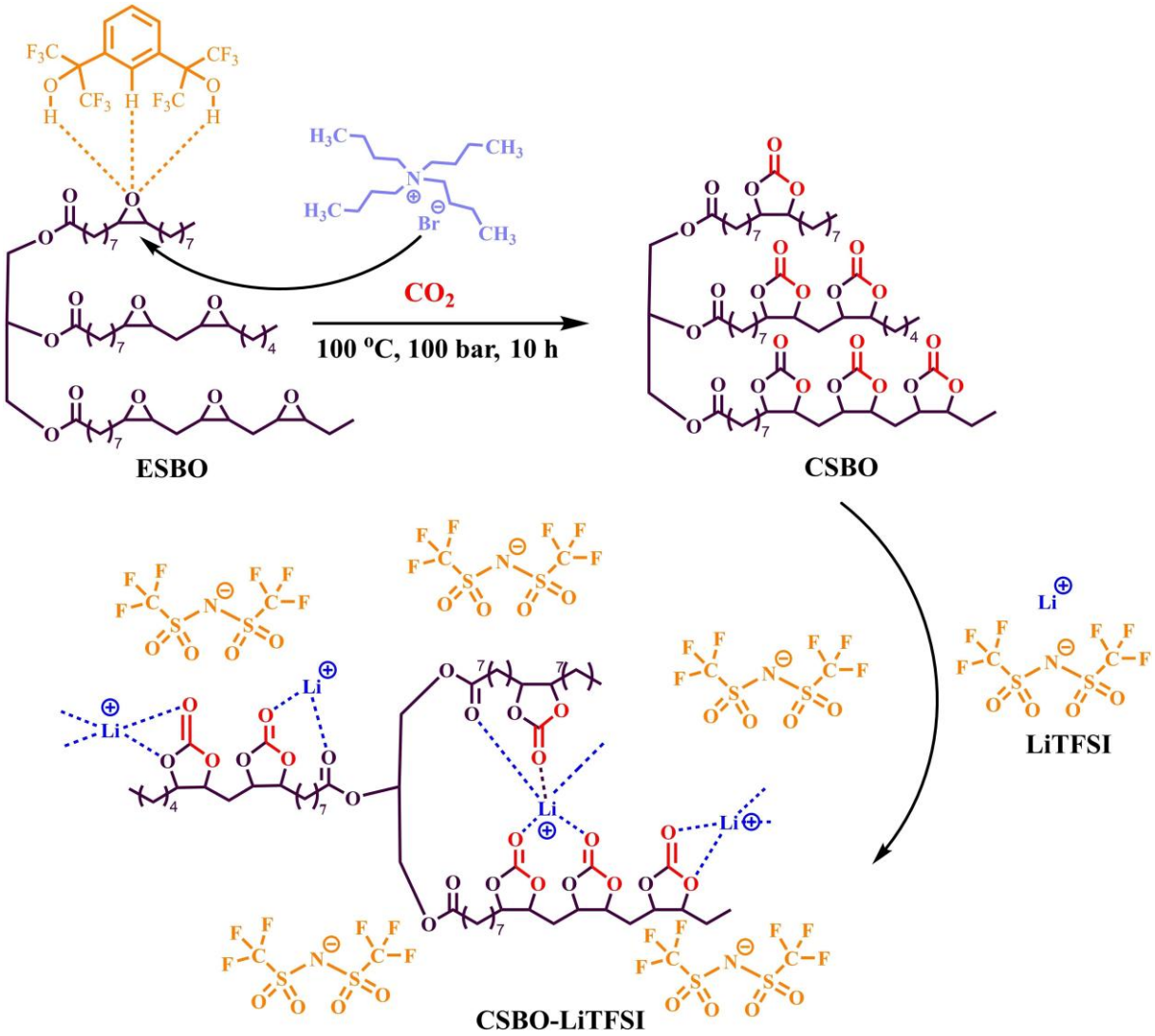

Scheme 1. *Synthesis of CSBO along with CSBO molecule interacting with LiTFSI.*

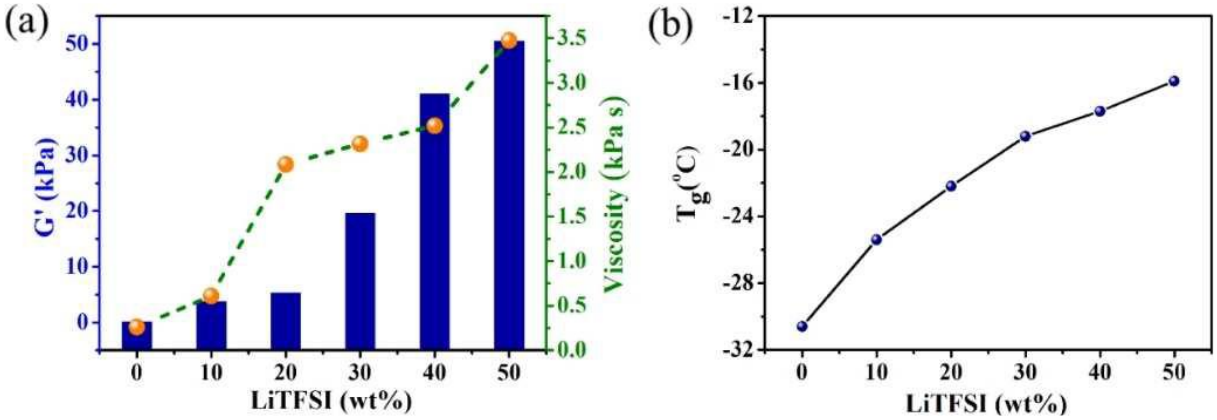

Figure 1. *(a) Storage modulus and viscosity at 25 °C and (b) glass transition temperatures (T_g) of CSBO-LiTFSI solid electrolytes with varying LiTFSI content (without cellulose/filter paper).*

Published in : ChemSusChem (2022), vol. 15, n°18, e202200913
DOI: doi.org/10.1002/cssc.202200913
Status : Postprint (Author's version)

Results and Discussion

MECHANICAL AND THERMAL PROPERTIES OF CSBO-LITFSI COMPOSITES

The synthesis and chemical structure of CSBO-LITFSI are depicted in Scheme 1. The successful transformation of epoxide groups into carbonate ones was evidenced by ^{1}H nuclear magnetic resonance (NMR) (Figure S1) and Fourier-transform infrared (FTIR) (Figure S2) spectroscopies. All the investigated CSBO-LiTFSI samples behaved as viscous liquids with a slight shear thinning behavior.[60] The influence of LiTFSI salt concentration on the shear behavior was investigated by measuring the complex viscosity at a frequency of 1 Hz (Figure 1a). The complex viscosity significantly increased with the amount of added LiTFSI. We assume that the interactions between Li^+ ions and cyclic carbonates groups in CSBO allow not only efficient dissolution of LiTFSI in CSBO (all the investigated samples looked homogeneous as an indication of efficient dissolution of LiTFSI in CSBO in various batches of samples), but also intermolecular interactions between CSBO molecules and stiffening of the CSBO molecules, both resulting in an increased viscosity. The amorphous nature of CSBO-LiTFSI samples was confirmed by differential scanning calorimetry (DSC) (Figure S3). Indeed, CSBO-LiTFSI samples only show a glass transition temperature (T_g), whose value is almost linearly increasing with the amount of added LiTFSI (Figure 1b). This can be related to the decreased mobility of aliphatic soft segments in CSBO with higher LiTFSI salt content in line with inter- and intramolecular Li^+/carbonate interactions as discussed above. In addition, the T_g remains always well below 0 °C even for the highest LiTFSI loading (50 wt %). A low T_g is essential for the adhesive nature of the material, which in turn facilitates good contact and wettability with the electrode interface.[61, 62] Nevertheless, since CSBO-LiTFSI mixtures are highly viscous liquids, they are too soft to form self-supporting membranes and to be used as such in solid-state batteries. This is the reason why solid electrolyte membranes (see further electrochemical characterizations) have been formed by casting the CSBO-LiTFSI mixtures directly in cellulose/filter paper, the latter playing the role of a mechanically supporting membrane or separator (see Experimental Section). Cellulose has indeed been selected as bio-based supporting materials. Thermogravimetric analysis (TGA) was performed to evaluate the thermal stability of CSBO-LiTFSI samples. There was almost no weight loss beyond around 144 and 193.33 °C for $CSBO_{40–50\%}$ (the numbers in subscript indicate the wt % of added LiTFSI and $CSBO_{0–30\%}$, respectively) (Figure 2). This initial weight loss prior to major decomposition can be attributed to the release of moisture traces trapped by the LiTFSI salt. The major decomposition starts at around 260 °C for the CSBO-LiTFSI samples and continues until around 475 °C. It is worth noting that the major decomposition was delayed at around 330 °C for the CSBO sample with no added LiTFSI. This can be explained by the weakening of C−O bonds in the carbonate groups as a result of O−Li^+ coordination.[63] Moreover, the introduction of LiTFSI in CSBO leads to a more complicated decomposition pathway compared to pure CSBO (Figure 2).

Published in : ChemSusChem (2022), vol. 15, n°18, e202200913
DOI: doi.org/10.1002/cssc.202200913
Status : Postprint (Author's version)

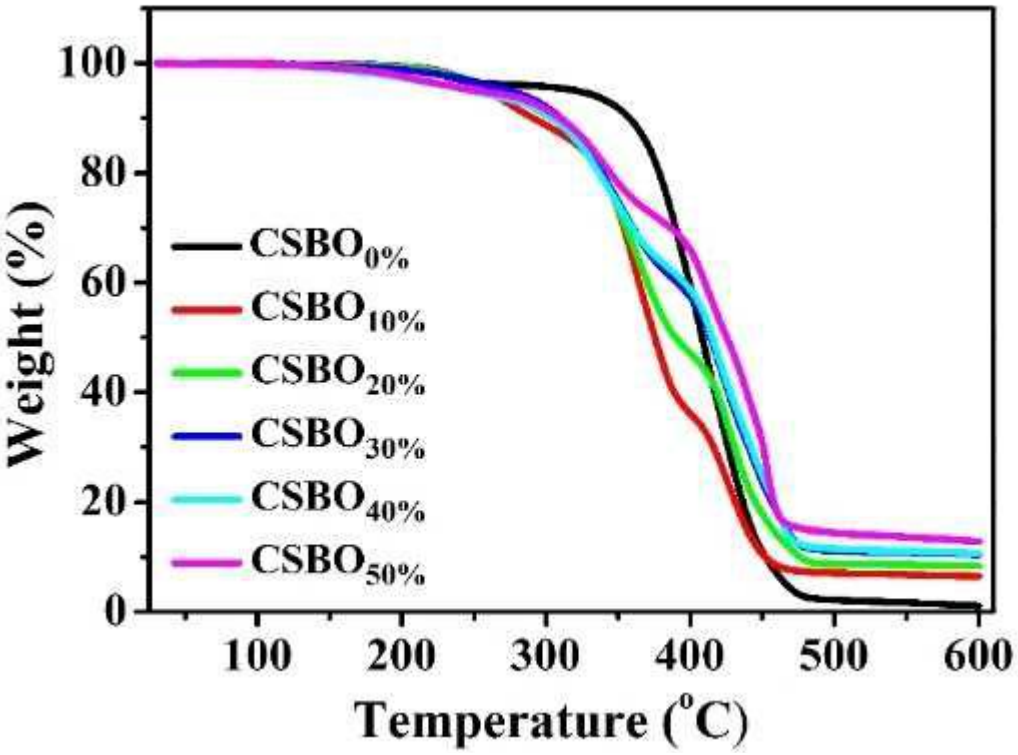

***Figure 2**. TGA of CSBO-LiTFSI samples.*

IONIC CONDUCTIVITY OF CSBO-LITFSI SOLID ELECTROLYTES

The temperature-dependent ionic conductivities of cellulose paper-supported CSBO-LiTFSI solid electrolytes with LiTFSI content varying from 10 to 50 wt % were investigated by potentiostatic electrochemical impedance spectroscopy (PEIS) and displayed in the form of Nyquist plots as shown in Figure 3a for 20 °C (and Figure S4 for 60 °C).

Published in : ChemSusChem (2022), vol. 15, n°18, e202200913
DOI: doi.org/10.1002/cssc.202200913
Status : Postprint (Author's version)

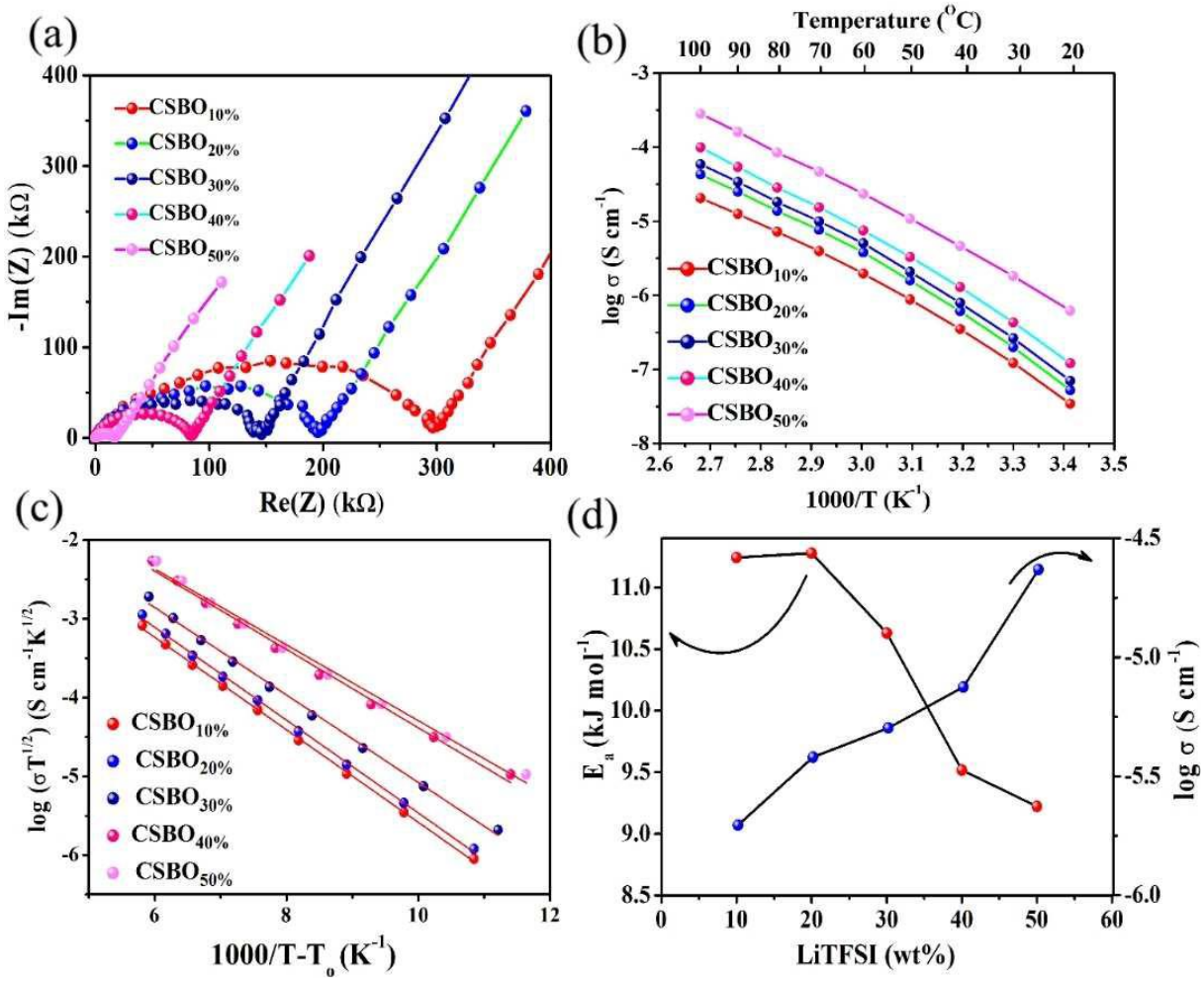

Figure 3. *(a) Nyquist plots of CSBO as a result of PEIS at 20 °C. (b) Temperature-dependent ionic conductivity for CSBO-LiTFSI (10–50 wt %) SEs (depicted as $CSBO_{x\%}$). (c) Temperature-dependent ionic conductivity using the Vogel–Fulcher–Tamman (VFT) model. (d) y1 axis as activation energy, E_a, derived using VFT equation from ionic conductivity plot and y2 axis as conductivity at 60 °C versus the wt % of LiTFSI in the SE.*

The ionic conductivities (σ) of CSBO-based SEs were calculated using Equation (1) :

$$\sigma = \frac{l}{RS} \quad (1)$$

where *R* is the bulk electrolyte ohmic resistance from AC impedance, and *l* and *S* are the thickness and the surface area of the analyzed polymer electrolyte thin film, respectively. As expected, the ionic conductivities of SEs were substantially increased with increasing temperature (20–100 °C) due to the enhanced mobility of fatty acid chain segments and charge carriers. The sample loaded with 50 wt % LITFSI displays the best value of ionic conductivity (≈10^{-3} S cm^{-1} at 100 °C and ≈10^{-6} S cm^{-1} at 20 °C), as depicted in Figure 3b. The obtained ionic conductivity data were averaged over 4–5 different membranes measurements and plotted with less than 4 % error. As already pointed above, our electrolyte system based on CSBO is able to dissolve a high amount of salts. The results are in agreement with previous studies on polyether- or polyester-based polycarbonates that provided the highest ionic conductivity at 30–36 wt % LITFSI.[43, 64, 65] The conductivity values seem to

Published in : ChemSusChem (2022), vol. 15, n°18, e202200913
DOI: doi.org/10.1002/cssc.202200913
Status : Postprint (Author's version)

align well with Arrhenius behavior following almost a linear regime upon the inverse of temperature. The conductivity data have also been fitted by using the Vogel–Fulcher–Tamman (VFT) equation [Eq. (2)] over the temperature range of 20–100 °C :

$$\sigma T^{1/2} = Ae^{-\frac{E_\alpha}{k_b (T-T_o)}} \quad (2)$$

where A is the pre-exponential factor, T is the absolute temperature, T_o is the Vogel scaling temperature at which the free volume disappears or at which free entropy becomes zero, T_o is related to T_g by T_g–50 K following an approximation,[66] E_α is the pseudoactivation energy of ion transport, and k_b is the Boltzmann constant.

The VFT model has been applied in order to demonstrate the effect of segmental motion on the overall conductivity above T_g.[67, 68] The activation energy calculated from the slope of VFT plot and Equation (2) is found to decrease with an increase in the salt content as shown in Figure 3d. This could be explained by the fact that, at higher salt content, ionic conductivity is not only solely based on ion-hopping of Li^+ ions from neighboring carbonate groups but also on diffusion of free ions dissolved in the fatty acid segments. The coupled effect of hopping and segmental motion in our system at a high percentage of salt could explain why less energy is required for the transport of ions under those conditions. Figure 3d shows the trend of activation energy E_a and ionic conductivity as a function of the weight percentage of LiTFSI salt derived from the results plotted in Figures 3b, c. Table 1 shows the E_a calculated for the CSBO-LiTFSI SEs with various LiTFSI loading along with the pre-exponential factor and R^2 as corresponding fitting coefficient.

CSBO-Li	T_g [°C]	R^2	ln$A$	E_a [kJ mol^{-1}]
10 %	−25.4	0.999	0.289	11.24
20 %	−22.2	0.999	0.427	11.28
30 %	−19.2	0.997	0.475	10.63
40 %	−17.7	0.992	0.588	9.52
50 %	−15.9	0.992	0.524	9.22

Table 1*. Activation energy and pre-exponential factor as calculated from the slope of VFT plots.*

LINEAR SWEEP VOLTAMMETRY OF CSBO-LITFSI SOLID ELECTROLYTES

Linear sweep voltammetry (LSV) measurements have been performed to investigate the electrochemical stability window (ESW) of the investigated of CSBO-LiTFSI SEs. The fabrication of the cell for LSV measurements is pictured in Figure 4a. The measurements were recorded on a wide voltage window of 0–5 V to probe the ESW with a scan rate of 0.5 mV s^{-1} versus Li/Li^+ at RT and 60 °C. The results reported in Figure 4b reveals that CSBO-LiTFSI SEs were electrochemically stable over 4.8 and 4.6 V (vs. Li/Li^+) at RT and 60 °C, respectively. However, a slightly higher cut-off current density has been observed in the case of $CSBO_{50\%}$ owing to higher salt content. In addition, the ESW of CSBO-LiTFSI SEs was significantly decreased with increasing temperature along with increased cut-off current density for higher LiTFSI loading. The electrolyte decomposition at higher voltage

Published in : ChemSusChem (2022), vol. 15, n°18, e202200913
DOI: doi.org/10.1002/cssc.202200913
Status : Postprint (Author's version)

was also cross-checked by changing the electrode from Al to Al-carbon foil and pure stainless-steel spacer (see Experimental Section), as shown in the Supporting Information (Figure S5). From all these data, we did not evidence any Al corrosion with LiTFSI even at the higher potential of 4.5–5.0 V. The high ESW indicates the electrolyte compatibility with Li-electrodes and no oxidation was observed on the cathodic side. Consequently, bio-based CSBO-LiTFSI SEs appeared as promising electrolytes compared to PEO-based SPE for lithium metal batteries in the operational window of most of standard commercial cathode materials.[69, 70]

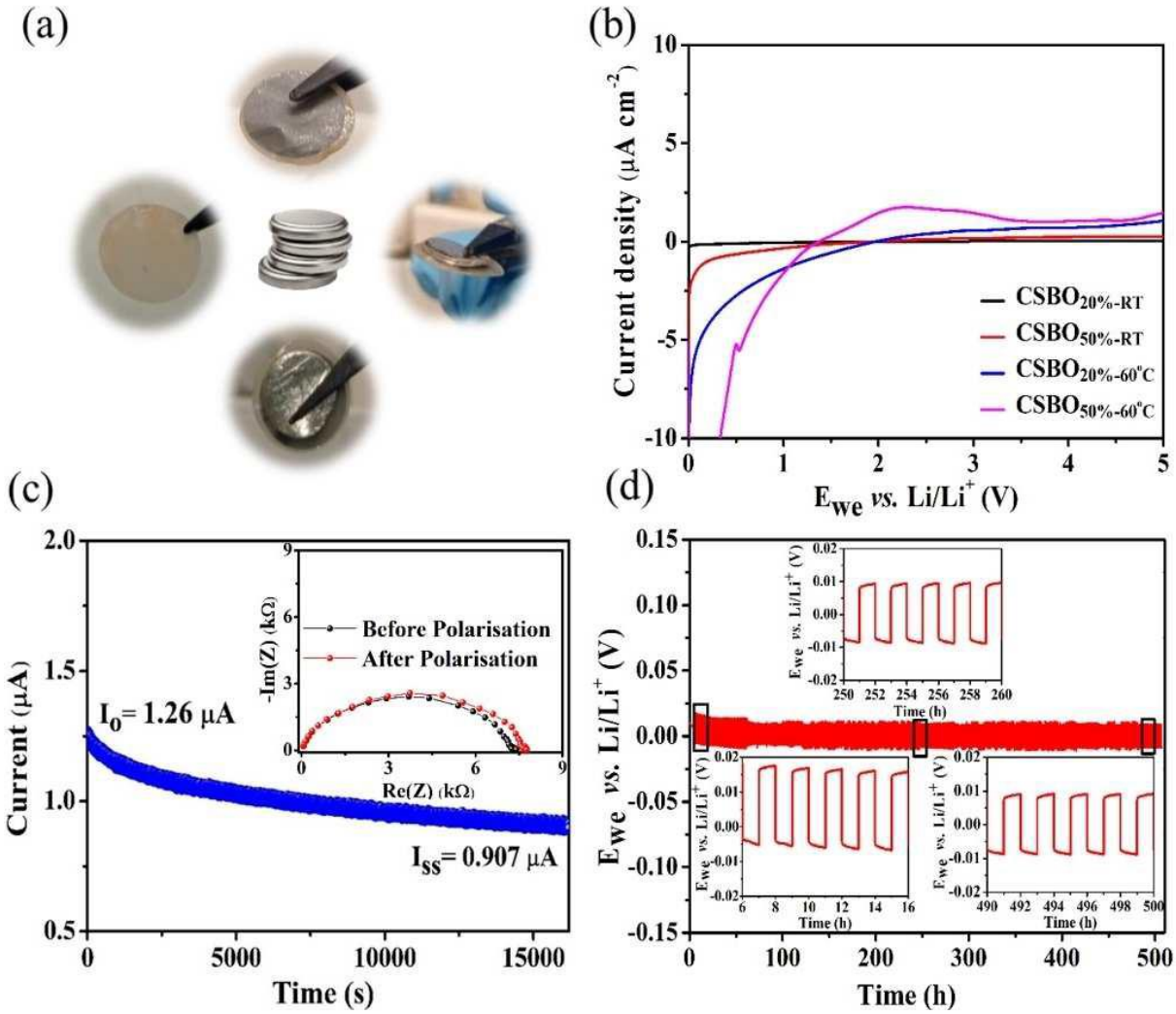

Figure 4. *(a) Cell fabrication for LSV measurements. (b) LSV of the $CSBO_{20\%}$-SE and $CSBO_{50\%}$-SE at RT and 60 °C with Al and lithium electrodes. (c) Chronoampereometry measurement at 10 mV for $CBSO_{50\%}$-SE with Nyquist plots for PEIS before and after polarization in the inset at RT. (d) Galvanostatic charge-dicharge for stripping and plating of lithium in Li|$CBSO_{50\%}$-SE|Li symmetric cell with three enlarged plots at respective time demonstrating the constant overpotential in the inset.*

Published in : ChemSusChem (2022), vol. 15, n°18, e202200913
DOI: doi.org/10.1002/cssc.202200913
Status : Postprint (Author's version)

TRANSFERENCE NUMBER OF CSBO-LITFSI SOLID ELECTROLYTES

The lithium transference number (t_{Li^+}) of a symmetric Li|CSBO$_{50\%}$-SE|Li cells was determined by AC impedance combined with DC polarization. The t_{Li^+} value was calculated using the Bruce–Vincent method,[71,72] following Equation (3) :

$$t_{Li^+} = \frac{I_{ss}(V - I_o R_o)}{I_o(V - I_{ss} R_{ss})} \quad (3)$$

where V is the DC applied potential, and I_o and I_{ss} are the initial and steady-state currents recorded with R_o and R_{ss} as initial and steady-state interfacial resistances from PEIS measurements at an AC sinusoidal voltage of 10 mV. Figure 4c shows that the polarization as a result of constant potential of 10 mV changes the interfacial resistance from 7350 to 7749 Ω, while current varies from an initial value of 1.26 µA to a stabilized value of 0.91 µA. The t_{Li^+} of CSBO$_{50\%}$ was then calculated to be 0.39±0.03 at 30 °C (t_{Li^+} =0.31±0.03 at 60 °C as in Figure S5d), in agreement with results previously reported by Han.[73] This value is comparable to the commercial liquid electrolytes (0.31) and higher than PEO-based polymer electrolytes (0.2).[73] A high t_{Li^+} is indeed a crucial parameter for the long-term cycling of batteries, allowing efficient diffusion and lower coulombic efficiency loss.

STRIPPING AND PLATING EXPERIMENTS FOR CSBO-LITFSI SOLID ELECTROLYTES

The time-dependent voltage profile was investigated on symmetric Li|CSBO$_{50\%}$-SE|Li cell using galvanostatic cyclic measurements at current densities of 0.4 µA cm^{-2} at RT. Reversible plating/stripping of Li-metal was carried out for a prolonged time for an individual plating or stripping steps with charge and discharge for 1 h each at RT for Li-symmetric cells and was recorded an average overpotential in the range of 150 to 200 mV during initial cycles. As it can be observed in Figure 4d, a slight overpotential is associated with the bulk resistance of the electrolyte and electrolyte/electrode interface.[74] As a result of multiple cycling, the SEI layer stabilizes and facilitates the mobility of Li^+ ions at the interfaces. Steady state was observed to be achieved in less than 100 h with more or less constant overpotential. These constant values are mirroring a high coulombic efficiency and reversibility in the electrochemical process with efficient Li-ion transport and stable interface that minimizes dendrites formation and growth. The constant overpotentials also confirm the formation of a stable and conducting SEI beneficial for a long cycling life of the cells.[1] As a result of minor fluctuations in cell temperature at RT, a slight increase in the overpotential is, however, recorded in day-night measurements. With these results, the good interfacial compatibility of the CSBO-LiTFSI SEs with Li-metal was revealed.

LI-METAL BATTERIES BASED ON CSBO-LITFSI SOLID ELECTROLYTES

In order to probe the applicability of our bio-based CSBO-LiTFSI SEs in all solid-state lithium metal batteries, battery prototypes constituting of a cathode based on $LiFePO_4$ (LFP), an anode of metal

Published in : ChemSusChem (2022), vol. 15, n°18, e202200913
DOI: doi.org/10.1002/cssc.202200913
Status : Postprint (Author's version)

Li, and CSBO-LiTFSI solid electrolytes have been constructed (abbreviated as LFP|$CSBO_{x\%}$-SE|Li) and their galvanostatic cycling performances have been measured at various temperatures with different concentration of salt-loaded CSBO electrolytes over multiple batch of samples. The cathode has been formulated from LFP as electroactive material, carbon as conducting agent, poly(vinylidene difluoride) (PVDF) as binder, and CSBO as catholyte for ion transport (see Experimental Section). CSBO-LiTFSI/cellulose SEs have been used as electrolyte membrane. It is clearly supported by the PEIS measurements on the Li metal battery prototypes (Figure 5a) that CSBO-LiTFSI/cellulose SEs with higher LiTFSI content are characterized by a higher conductivity and will lead to better performance for the battery. Indeed, the $CSBO_{50\%}$-SE with the highest LiTFSI content shows a semi-circle in the Nyquist plot that correlates with an electric double layer capacitive behavior (Figure 5a). The enhancement in the diffusion of Li^+ ion in the electrolyte to electrode interface for this electrolyte can be noted from the inclination of Warburg impedance away from the real resistance axis (subset of Figure 5a). In contrast, it was observed that the cells made with CSBO-LiTFSI/cellulose SEs with lower LiTFSI content ($CSBO_{20–40\%}$) could not deliver decent specific capacity at RT at 0.1 C rate due to insufficient lithium-ion conductivity and transport.

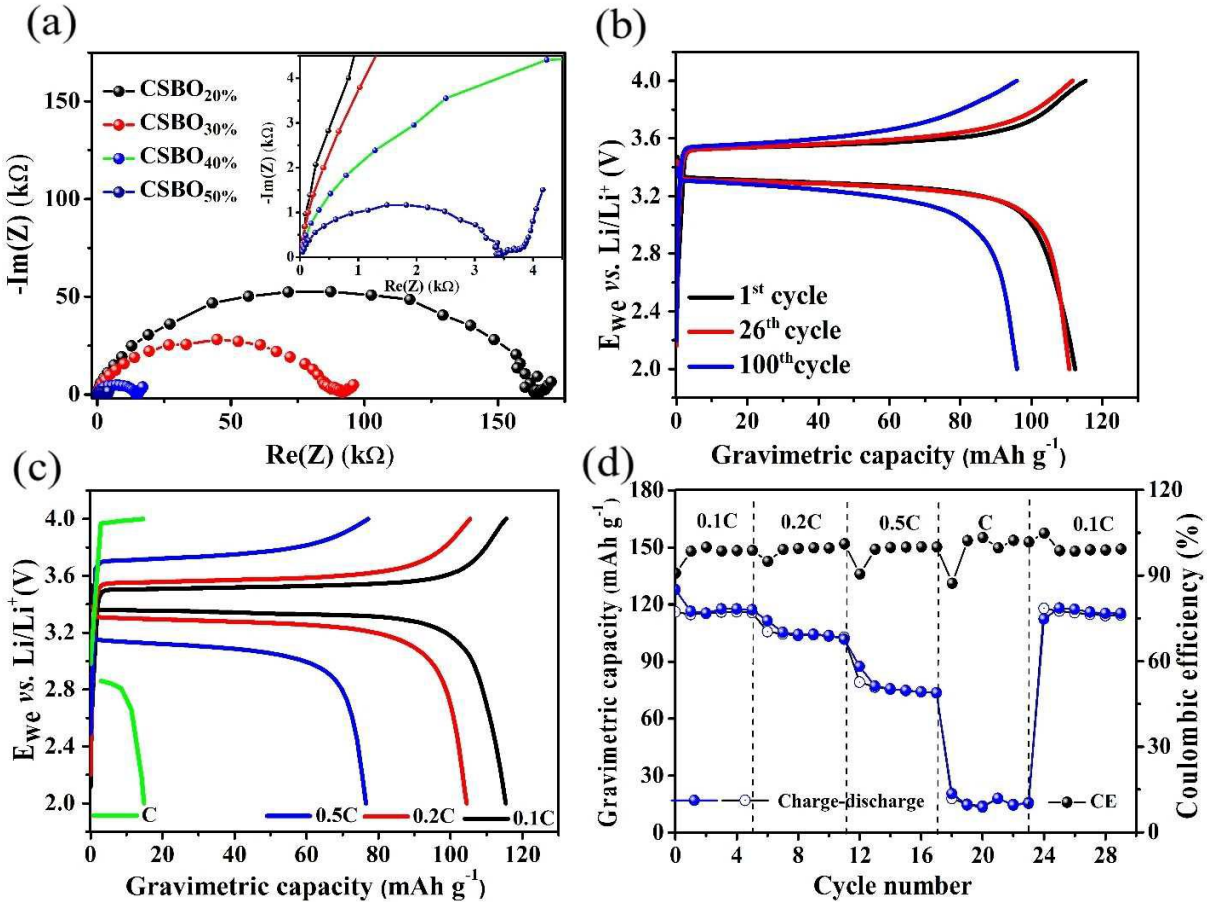

Figure 5. *(a) Nyquist plot of Li|$CSBO_{x\%}$-SE|LFP at RT with enlarged PEIS of Li|$CSBO_{50\%}$-SE|LFP. (b) Galvanostatic charge-discharge voltage profile at 0.1 C. (c) Galvanostatic charge-discharge voltage profile at different C-rate. (d) Rate capability plot of Li|$CSBO_{50\%}$-SE|LFP at RT.*

Published in : ChemSusChem (2022), vol. 15, n°18, e202200913
DOI: doi.org/10.1002/cssc.202200913
Status : Postprint (Author's version)

Figure 5b shows galvanostatic charge-discharge voltage profile of the LFP|$CSBO_{50\%}$-SE| Li cell with obtained capacity of 124 and 112 mAh g^{-1} in 1st charge and discharge cycle, respectively, at the 0.1 C-rate at RT. The oxidation and reduction plateau for LFP has been observed at 3.52 and 3.32 V approximately without significant polarization in subsequent 26th and 100th cycles. However, galvanostatic charge-discharge curves at different C-rates show a drastic polarization at a higher current density. Similarly, the change in oxidation potential, ΔE_{OO} and change in reduction potential, ΔE_{RR} for the corresponding charge-charge and discharge-discharge at 0.1 and 1 C were observed to increase by 0.47 and 0.51 V, respectively. The ΔE_{OR} between oxidation and reduction increased from 0.15 V at 0.1 C to 1.18 V at 1 C, as seen in Figure 5c. This phenomenon correlates to nothing but the poor conductivity at the interface between electrode and electrolyte. Nonetheless the charge-discharge at RT is achievable due to current density in rate capability plot measurements (Figure 5d), indicating that the cell regains back its capacity at 0.1 C rate even after a significant capacity loss at 1 C rate. The capacity retention was calculated to be 83 % for long-term cycling with a capacity of 96 mAh g^{-1} at the 100th cycle, as shown in Figure 6d.

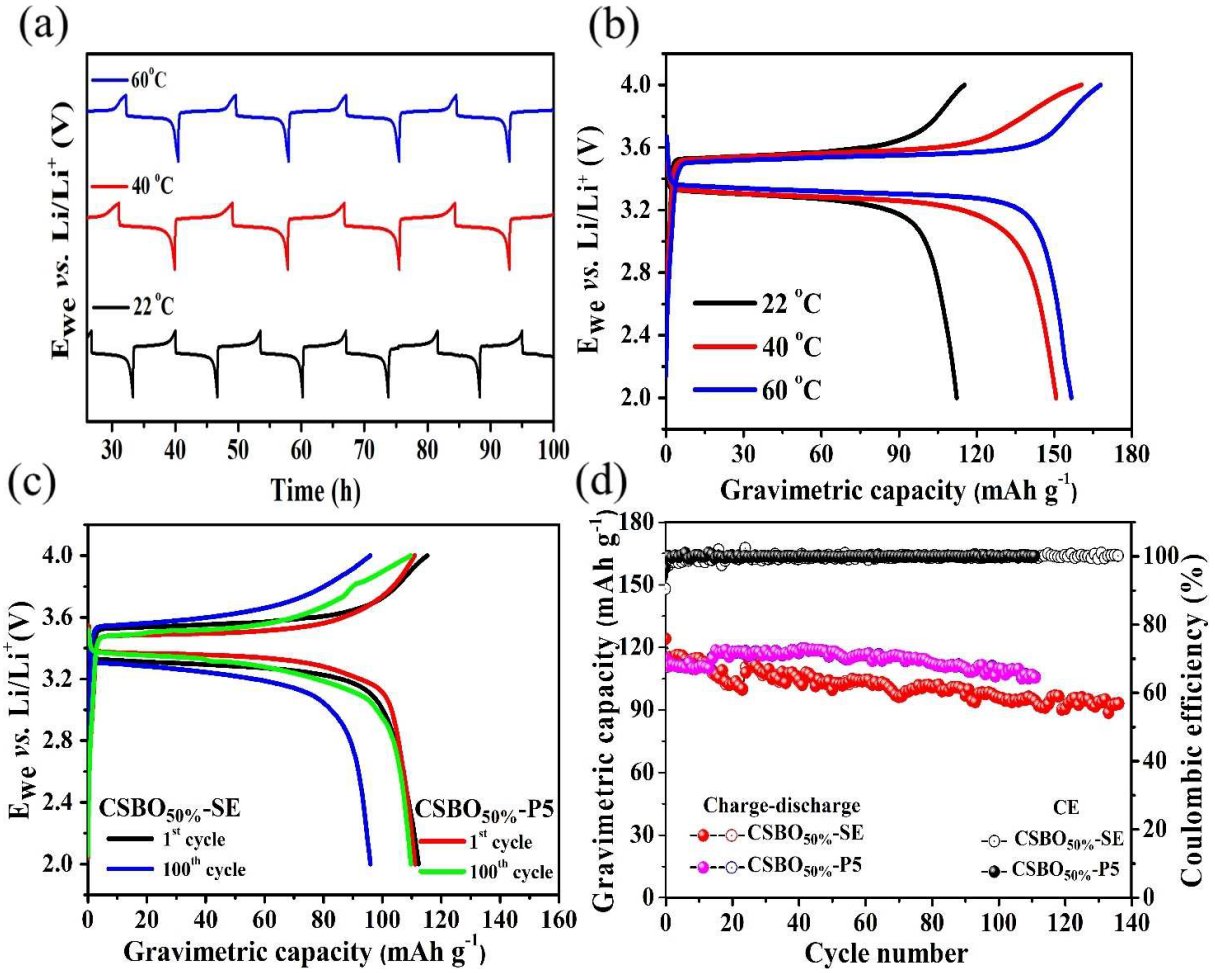

Figure 6. *Galvanostatic charge-discharge voltage profile with respect to (a) time and (b) with gravimetric capacity at 0.1 C for Li|$CSBO_{50\%}$-SE|LFP at variable temperature. (c) Galvanostatic charge-discharge voltage profile with gravimetric capacity for 1st and 100th cycle and (d) capacity retention plot with cycle number for Li|$CSBO_{50\%}$-SE|LFP and Li|$CSBO_{50\%}$-P5|LFP at 0.1 C at RT.*

Published in : ChemSusChem (2022), vol. 15, n°18, e202200913
DOI: doi.org/10.1002/cssc.202200913
Status : Postprint (Author's version)

Although the experimental capacity for LFP obtained for the LFP|CSBO$_{50\%}$-SE|Li cell is not reaching the theoretical capacity of LFP, it constitutes a very promising result in the context of solid-state lithium metal batteries without the use of plasticizers, additives, or elevated temperature.[75, 76] In order to increase the performance of our system, we first increase the temperature of operation of our LFP|CSBO$_{50\%}$-SE|Li cell. As shown in Figure 6a, the increase in charging and discharging time with increasing temperature is self-explanatory. As the temperature increases, the mobility of fatty chain segments in CSBO along with the increased mobility of ions contribute to the improvement of the overall experimental capacity. With the LFP|CSBO$_{50\%}$-SE|Li cell, we are able to achieve a discharge capacity as high as 157 mAh g^{-1} at 60 °C in comparison to 151 and 112 mAh g^{-1} at 40 °C and RT, respectively (see also Figure S6 for rate capability and capacity retention at 60 °C).

Another possibility to increase the cell performance is by the inclusion of plasticizer in the SE. Here, we have selected propylene carbonate (PC) as plasticizer because PC is fully miscible with the CSBO-LiTFSI-SE. The role of the plasticizer is to enhance mobility and transport of ions.[77-79] Figure S7c shows the effect of the amount of plasticizer on charge-discharge performance at 0.1 C. According to the data shown in Figure S7, it seems that an added around 5 wt % of PC to CSBO$_{50\%}$ (5 µL by volume, represented by P5) is sufficient to significantly increase the cell performance. Figure 6c shows galvanostatic charge-discharge curves for the LFP|CSBO$_{50\%}$-SE|Li cell (without P5) and Li|CBSO$_{50\%}$-P5|LFP with P5. Although there is no enhanced capacity during the first cycle due of the presence of plasticizer, a visible improvement in the capacity can be observed for the 100th cycle for the CBSO$_{50\%}$-P5 cell. In addition, the ΔE_O and ΔE_R for LFP were found to be decreased upon addition of plasticizer from 3.52 to 3.47 V and 3.37 to 3.32 V for oxidation and reduction, respectively. Moreover, during the subsequent 100th cycle, the $\Delta E_{OO}/\Delta E_{RR}$ in respective charge or discharge is observed to be around 0.02 V for CBSO$_{50\%}$-SE and less than 0.005 V for CSBO$_{50\%}$-SE-P5. This is also fully supported by a lower electrolytic bulk resistance recorded in the PEIS measurements of the respective cells as shown in Figure S6. Figure 6d shows the comparison in the capacity retention of the CSBO$_{50\%}$-SE and CSBO$_{50\%}$-P5 cells. The capacity retention is enhanced from 83 to 96 % with P5 coulombic efficiencies for both ranging in between 99–100 %. In contrast, there is no improvement in the overall capacity with P5 plasticizer in comparison to P10 and P20 (P10 and P20 correspond to 9.7 and 17.8 wt % of PC, 10 and 20 µL of PC by volume for CSBO$_{20\%}$) as recorded (see Figures S7 and S8).

POST-CYCLING XPS ANALYSIS OF ELECTRODE INTERFACES

For a stable electrolyte, minimal growth of dendrite or its suppression (if any) are crucial parameters for a longer performance of the battery. The active formation of lithium fluoride (LiF) in an SEI layer as a result of the decomposition of LiTFSI serves the purpose of ensuring efficient Li-ion mobility while limiting the dendrite growth.[80, 81] Therefore, X-ray photoelectron spectroscopy (XPS) measurements on the surface of the Li anode and LFP cathode for Li|CSBO$_{50\%}$-SE|LFP cells were performed to probe the interfacial composition after galvanostatic charge-discharge for more than 100 cycles at 0.1 C. The C 1s peak at 284.8 eV was used as a reference to calibrate the binding energy.[82] The major C and O elements could not be ignored from the XPS chamber or atmosphere

Published in : ChemSusChem (2022), vol. 15, n°18, e202200913
DOI: doi.org/10.1002/cssc.202200913
Status : Postprint (Author's version)

and hence can also correspond to adventitious carbon. The survey spectra detected the desired elements like C, O, Li, F, N, S, and P originating from the SEI layer or the other constituents from electrodes, as shown in Figure 7a. The abundance ratio percentage of functional carbons and elements has been presented through the bar charts in Figure 7b, c.

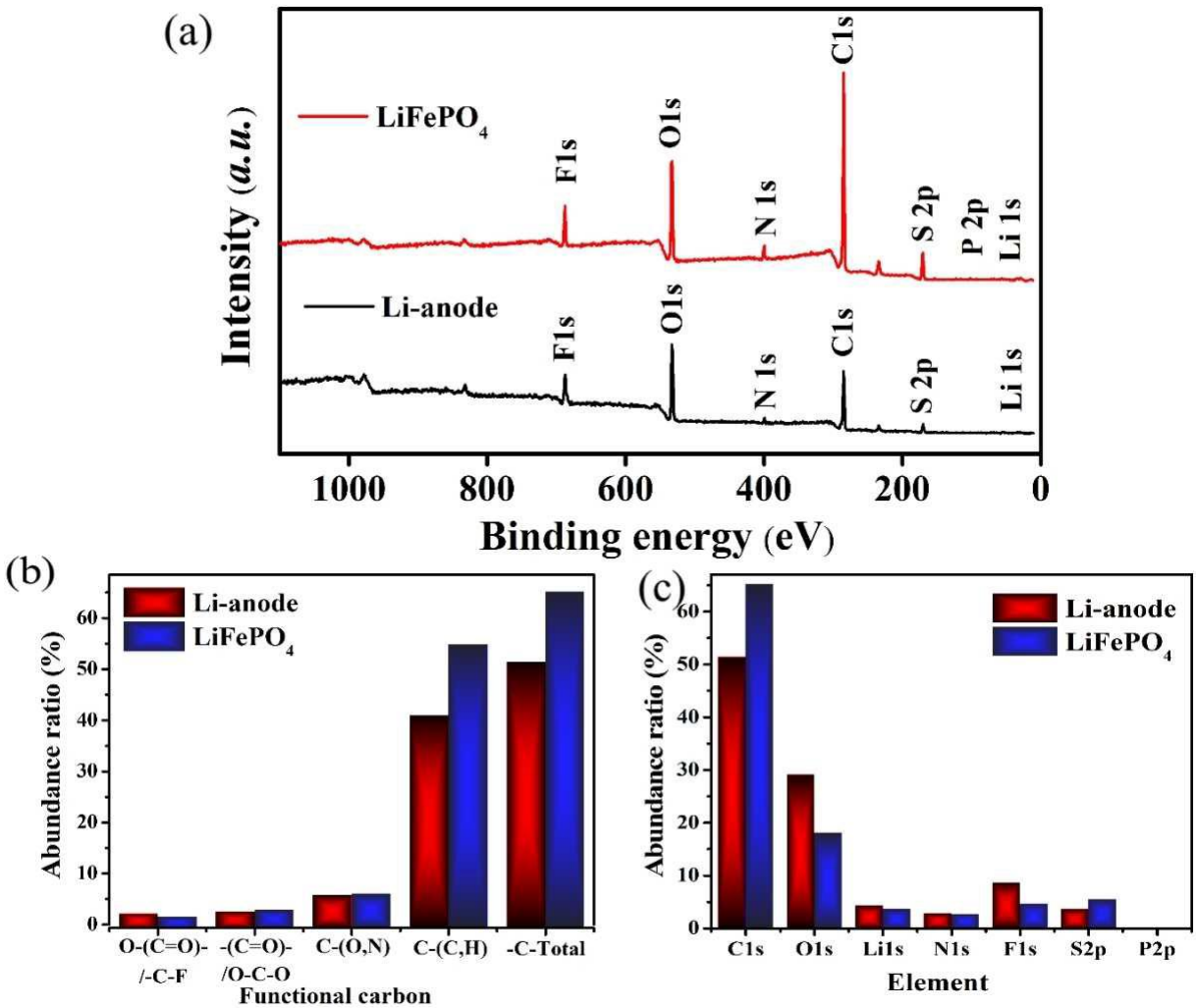

Figure 7. *(a) Survey spectrum of LFP cathode and lithium metal anode after cycling for more than 100 cycles of Li|CSBO$_{50\%}$-SE|LFP. (b) Bar charts showing the abundance ratio percentage of functional carbon and (c) elements from their surface.*

The C 1 s spectra in both samples can be attributed to C−C/C−H, C−O/N, and O−C−O/C=O with the binding energy of around 284.8, 286.3, and 287.8 eV, respectively. Other O−(C=O)−/−C−F functional species have been detected at 289.54 and 289.98 eV for Li-metal surface and LFP with a shift of 0.44 eV, as shown in Figure 8a, d. As a result of prolonged cycling, a significant amount of 2.6 % LiF species in the F 1s spectra (Figure 8b) at the binding energy of 684.8 eV was detected at the surface of the Li anode, in agreement with the formation of a stable SEI.[83] 6.1 and 4.6 % −CF_3 derived from LiTFSI were recorded at 687.6 and 687.8 eV for Li anode and LFP cathode, respectively (Figure 7c and Table S1). The S 2p spectra in Figure 8c, d show the characteristic peaks of sulfone (−SO_x) from LiTFSI for both electrodes. The high-resolution (HR)-XPS of O 1s could not be deconvoluted owing to overlapped peaks which may correspond to the following species, S−O (LiTFSI), O−(C=O)−O,

Published in : ChemSusChem (2022), vol. 15, n°18, e202200913
DOI: doi.org/10.1002/cssc.202200913
Status : Postprint (Author's version)

O−(C=O)−C, C−OH, and C−(SO_2) (Figure S9, also showing Li 1s, N 1s, and P 2p XPS spectra). These insights complemented the good performance of our bio-based CSBO-SE-based Li-metal batteries by confirming the presence of LiF species for a stable SEI.

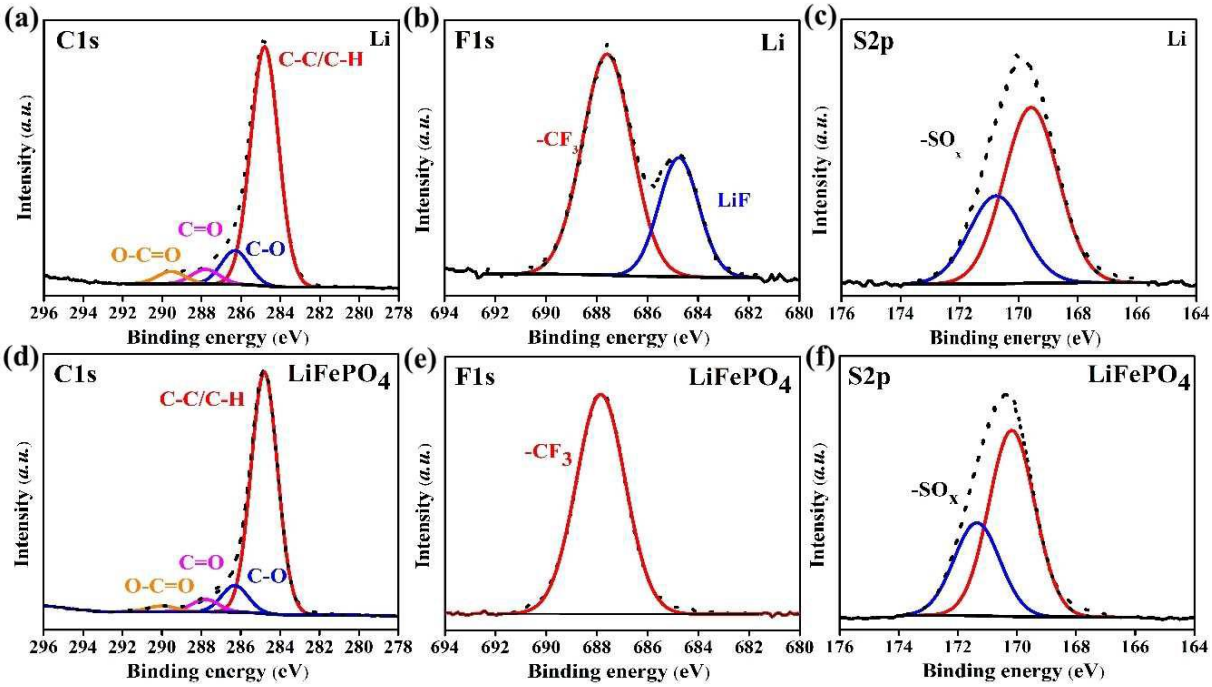

Figure 8. *HR-XPS of (a, d) carbon (C 1s), (b,e) fluorine (F 1s) and (c, f) sulfur (S 2p) for lithium metal and LFP surface of cycled Li|$CSBO_{50\%}$-SE|LFP cell, respectively.*

Conclusion

In this contribution, we have disclosed an approach to develop solid electrolytes from bio-based starting materials (namely carbonated soybean oil and cellulose) and CO_2 using a green chemistry approach. The carbonated soybean oil (CSBO) was capable of dissolving lithium salts, thanks to its high dielectric constant resulting from the presence of cyclic carbonate groups. As anticipated, the ionic conductivities of CSBO-LiTFSI [LiTFSI=lithium bis(trifluoromethanesulfonyl)imide] solid electrolytes (SEs) were substantially increased with the amount of added salt due to the increased number of charge carriers and temperature due to the enhanced mobility of chain segments. A maximum ionic conductivity of around 10^{-3} S cm^{-1} was obtained for $CSBO_{50\%}$ at 100 °C and 10^{-6} S cm^{-1} at 20 °C. Electrochemical stability window up to 4.8 V (vs. Li/Li^+) and lithium-ion transference number up to 0.39±0.03 were obtained for the $CSBO_{50\%}$-based SE at RT. However, our fundamental understanding of ionic transport in this system remains limited. Further electrochemical studies like galvanostatic charge-discharge measurements confirmed the stable solid electrolyte interphase (SEI) layer formation in subsequent stripping and plating. The CSBO-LiTFSI SEs were then incorporated in lithium metal battery cells using $LiFePO_4$ (LFP) as cathode material. The accordingly obtained cell can deliver up to 112 mAh g^{-1} of discharge capacity at 0.1 C, RT. The capacity of the cell was further shown to improve with parameters like elevated temperature and

Published in : ChemSusChem (2022), vol. 15, n°18, e202200913
DOI: doi.org/10.1002/cssc.202200913
Status : Postprint (Author's version)

addition of plasticizers to 156 mAh g^{-1} close to the theoretical capacity. Further, X-ray photoelectron spectroscopy on the Li-metal and LFP surface highlighted the stable SEI formation and decomposition of electrolyte. Our findings are paving the way towards bio-based and more environmentally friendly solid-state batteries operating at RT with the aim of high energy density.

Experimental Section

CHEMICALS

Epoxidized soybean oil (ESBO) was kindly donated by Vandeputte Oleochemicals (Belgium). Carbon dioxide (CO_2, N48) was supplied by Air Liquide. 1,3-Bis (2 hydroxyhexafluroisopropyl) benzene was purchased from Fluorochem. Tetrabutylammonium bromide (TBAB, >99 %), bis(trifluoromethane)sulfonimide lithium (LiTFSI), and cellulose separator [TF48-50 (50 µm×66 mm)] were purchased from Sigma Aldrich and TOB, respectively. Propylene carbonate (PC) was purchased from Sigma Aldrich. All reactants and catalysts were used as received, without any further purification.

CHARACTERIZATION TECHNIQUES

FTIR spectroscopy: FTIR measurements were carried out on a Nicolet IS5 spectrometer (Thermo Fisher Scientific) equipped with a diamond attenuated transmission reflectance (ATR) device. 32 Scans were recorded for each sample for different batches over the range of 4000–500 cm^{-1} with a normal resolution of 4 cm^{-1} and spectra were analyzed with the ONIUM™ software.

DSC: DSC analysis was carried out on a Q1000 TA Instruments using standard aluminum pans, calibrated with indium and nitrogen was used as a purge gas. The samples were analyzed at a heating rate of 10 °C min^{-1} over a temperature range from −80 to 200 °C under N_2 atmosphere, and the analysis was repeated three more times.

TGA: TGA was carried out using a Q500 from TA Instruments. Thermal degradation of samples was measured at a heating rate of 20 °C min^{-1} over the temperature range of 0 to 600 °C under a N_2 atmosphere.

Rheology: Rheological properties of samples were measured on an ARES (Advanced Rheometric Expansion System) Rheometric Scientific rheometer, equipped by two parallel plates geometry at a frequency (1 Hz), a strain (1 %), and the measurements were carried out at 25 °C. The evolutions of storage modulus and complex viscosity were monitored as a function of angular frequency.

XPS: XPS was performed using an SSI X-Probe (SSX 100/206) photoelectron spectrometer from Surface Science Instruments equipped with a monochromatized Al K_α (200 W) X-ray source. The batteries were disassembled, and samples were mounted on an XPS sample holder in a glovebox prior to transferring to the XPS vacuum chamber in the flux of argon atmosphere. All of the binding energies were calculated according to the C−(C, H) component of the C 1s peak fixed at 284.8 eV.

Published in : ChemSusChem (2022), vol. 15, n°18, e202200913
DOI: doi.org/10.1002/cssc.202200913
Status : Postprint (Author's version)

Data analysis was carried out using CasaXPS software. For the survey scan, a 1.0 eV step size was used and a 0.1 eV step size was used for high-resolution scans for all elements with 150 energy steps. Multiple samples were analyzed to validate data.

ELECTROCHEMICAL ANALYSIS

Electrochemical analysis of PEIS, LSV, chronoamperometry (CA), and galvanostatic cycling potential limitation (GCPL) were carried out on Biologic BCS-COM and VMP3 multichannel potentiostats using CR2032 coin cells.

PEIS: Ionic conductivity of CSBO SEs was determined by PEIS for symmetric stainless steel (SS|SE|SS) coin cells in the frequency range of 7 MHz to 50 mHz, with applied single sinusoidal A.C. excitation voltage of 10 mV. The temperature dependence measurements were carried out from 20 to 100 °C by gradually increasing temperature at the rate of 0.33 °C min^{-1}. 1 h was waited between each measurement to reach an equilibrium state. The experiments were repeated for several cells over different batches to optimize and avoid any errors.

LSV: Measurements were performed at various temperatures on asymmetric CR2032 coin cell as (Li|$CSBO_{x\%}$-SE|Al), (Li|$CSBO_{x\%}$-SE|Al-C|), and (Li|$CSBO_{x\%}$-SE|SS), over the potential range of 0–5 V (vs. Li/Li^+) at the scan rate of 0.5 mV s^{-1} at 30 and 60 °C over a few times.

t_{Li^+}: Transference number measurements were carried out on symmetric lithium metal cells (Li|$CSBO_{x\%}$-SE|Li) fabricated over various membranes by following the Bruce–Vincent method. Chronoamperometry with D.C. voltage of 10 mV was performed followed by PEIS measurements in the frequency range of 7–50 mHz, at 10 mV of A.C. excitation voltage at 30 and 60 °C. PEIS measurements were recorded before and after steady-state (before and after polarization).

GCPL: Galvanostatic charge-discharge cycling and rate capabilities measurement for the LFP|$CSBO_{x\%}$-SE|Li and LFP|$CSBO_{x\%}$-SE-P*X*|Li cells were tested with a Biologic BCS-COM cycler for various batches of electrolytes at different temperatures with and without plasticizers. The slurries for the cathodes were prepared from $LiFePO_4$, Super P, PVDF, CSBO, and *N*-methyl pyrrolidone (NMP) via grinding using a mortar pestle and were further casted on carbon-coated Al-foils using the doctor-blade technique. The coated slurries were then dried in an air oven for more than 6 h at 60 °C prior to vacuum drying at 120 °C for more than 24 h. The cathode components were maintained in the weight ratio of 7 : 2 : 1 and 5 : 2 : 1 : 2 for LFP, Super P and PVDF without CBSO and with CBSO slurries, respectively, after several trials. The cathodes and anodes were cut into disks of 14 mm diameter for the electrolyte membranes of 16 mm in diameter for the cell assembly.

SYNTHESIS OF CSBO

Bio-based CSBO was synthesized by reacting supercritical CO_2 with ESBO using a bicomponent organocatalytic system that combined TBAB as catalyst and 1,3-bis(2-hydroxyhexafluroisopropyl) benzene (HFI) as an activator as reported elsewhere by our group.[61, 84-86] The coupling reaction was

Published in : ChemSusChem (2022), vol. 15, n°18, e202200913
DOI: doi.org/10.1002/cssc.202200913
Status : Postprint (Author's version)

performed at 100 °C and 100 bar using 2.5 wt % of organocatalyst (TBAB/HFI molar ratio of 1) for 10 h. These optimized reaction conditions ensured the fast and full conversion of epoxy into corresponding cyclic carbonates. In a typical experiment, ESBO (30 g), TBAB (0.75 g, 2.32 mmol), and HFI (0.57 mL, 2.32 mmol) were introduced in an 80 mL high-pressure cell equipped with a mechanical stirrer. The cell was closed, the temperature and pressure were equilibrated at 100 °C and 100 bar for 10 h. After reaction, the pressure was released through the outlet and a viscous product was recovered. The conversion of ESBO into CSBO was investigated by ^{1}H-NMR spectroscopy (Figure S1) by the disappearance of the characteristic peaks of epoxides, −CH−O− and −CH_2−O− at 2.7 and 3.2 ppm, respectively. New peaks attributed to −CH−O−C(=O)O− and −CH_2−O−C(=O)O− cyclic carbonates appeared at 4.5 and 5.0 ppm, respectively. The formation of cyclic carbonates was further confirmed by FTIR spectroscopy (Figure S2) by the disappearance of the characteristic band of the epoxy groups of ESBO at 914 cm^{-1} and the presence of a new band at 1790 cm^{-1} corresponding to the carbonyl group of CSBO.

PREPARATION OF SOLID ELECTROLYTES

SEs were prepared from CSBO loaded with various amount of LiTFSI by a one-pot process. Prior to preparing the formulation, CSBO was degassed by thermal treatment at 70 °C overnight in a vacuum oven. CSBO (1.0 g, 0.8 mmol, cyclic carbonate average content per molecule=6, molar mass approximated to 1250 g mol^{-1})[87-91] was dissolved in DMC or THF (0.75 mL) and loaded with different amounts of LiTFSI (0–50 wt %). The obtained viscous solutions were drop-casted on cellulose support and then dried in a vacuum oven at 60 °C for more than 12 h and later at 60 °C for 5 h in the glovebox. The cellulose support allowed the formation of self-standing SE membranes containing 9.9 wt % of $CSBO_{50\%}$-SE.

Acknowledgements

A.R. and J.F.G. are grateful to INNOVIRIS for supporting this research in the frame of the BRIDGE FUSE project (2019-RPF-8). B.G. and C.D. thank the "Fonds National pour la Recherche Scientifique" (F.R.S.-FNRS) and the Fonds Wetenschappelijk Onderzoek – Vlaanderen (FWO) for financial support in the frame of the EOS project n°O019618F (ID EOS: 30902231). C.D. is F.R.S. – FNRS Research Director.

Conflict of interest

The authors declare no conflict of interest.

Published in : ChemSusChem (2022), vol. 15, n°18, e202200913
DOI: doi.org/10.1002/cssc.202200913
Status : Postprint (Author's version)

Data Availability Statement

The data that support the findings of this study are available from the corresponding author upon reasonable request.

References

[1] M. D. Murbach, D. T. Schwartz, *J. Electrochem. Soc.* 2018, *165*, A297.

[2] M. Armand, J. .-M. Tarascon, *Nature.* 2008, *451*, 652.

[3] J. W. Choi, D. Aurbach, *Nat. Rev. Mater.* 2016, *1*, 16013.

[4] A. Manthiram, X. Yu, S. Wang, *Nat. Rev. Mater.* 2017, *2*, 16103.

[5] K. J. Harry, D. T. Hallinan, D. Y. Parkinson, A. A. MacDowell, N. P. Balsara, *Nat. Mater.* 2014, *13*, 69.

[6] C. Wacker, *Annual Report*, *Fraunhofer ISIT*, Itzehoe, Germany, 2004. (https://www.ise.fraunhofer.de/content/dam/ise/en/documents/annualreports/ISE JB04 e Complete screen.pdf).

[7] Y. Yamada, J. Wang, S. Ko, E. Watanabe, A. Yamada, *Nat. Energy* 2019, *4*, 269–280.

[8] J. Lopez, D. G. Mackanic, Y. Cui, Z. Bao, *Nat. Rev. Mater.* 2019, *4*, 312–330.

[9] S. Choudhury, S. Stalin, D. Vu, A. Warren, Y. Deng, P. Biswal, L. A. Archer, *Nat. Commun.* 2019, *10*, 4398.

[10] J. Dai, C. Yang, C. Wang, G. Pastel, L. Hu, *Adv. Mater.* 2018, *30*, 1802068.

[11] L. P. Li, W. Y. Liu, H. Y. Dong, Q. Y. Gui, Z. Q. Hu, Y. Y. Li, J. P. Liu, *Adv. Mater.* 2021, *33*, 2004959.

[12] L. Bekaert, A. Raj, J.-F. Gohy, A. Hubin, F. D. Proft, M. H. Mamme, *J. Phys. Chem. C* 2022, *126*, 8227–8237.

[13] F. Elizalde, J. Amici, S. Trano, G. Vozzolo, R. Aguirresarobe, D. Versaci, S. Bodoardo, D. Mecerreyes, H. Sardon, F. Bella, *J. Mater. Chem. A* 2022, *10*, 12588–12596.

[14] X. Guo, Y. Ding, L. Xue, L. Zhang, C. Zhang, J. B. Goodenough, G. Yu, *Adv. Funct. Mater.* 2018, *28*, 1804649.

[15] R. Narayan, C. Laberty-Robert, J. Pelta, J. .-M. Tarascon, R. Dominko, *Adv. Energy Mater.* 2022, *12*, 2102652.

[16] D. H. Cho, K. G. Cho, S. An, M. S. Kim, H. W. Oh, J. Yeo, W. C. Yoo, K. Hong, M. Kim, K. H. Lee, *Energy Storage Mater.* 2022, *45*, 323–331.

[17] Y. Gao, Z. Pan, J. Sun, L. Zhaolin, W. John, *Nano-Micro Lett.* 2022, *14*, 94.

[18] Y. Tian, G. Zeng, A. Rutt, T. Shi, H. Kim, J. Wang, J. Koettgen, Y. Sun, B. Ouyang, T. Chen, Z. Lun, Z. Rong, K. Persson, G. Ceder, *Chem. Rev.* 2021, *121*, 3, 1623–1669.

Published in : ChemSusChem (2022), vol. 15, n°18, e202200913
DOI: doi.org/10.1002/cssc.202200913
Status : Postprint (Author's version)

[19] J. Amici, C. Torchio, D. Versaci, D. Dessantis, A. Marchisio, F. Caldera, F. Bella, C. Francia, S. Bodoardo, *Polymer* 2021, *13*, 1625.

[20] H. Oubaha, J.-F. Gohy, S. Melinte, *ChemPlusChem* 2019, *84*, 1179.

[21] J. Hassoun, B. Scrosati, *J. Electrochem. Soc.* 2015, *162*, A2582.

[22] K. Kubota, M. Dahbi, T. Hosaka, S. Kumakura, S. Komaba, *Chem. Rec.* 2018, *18*, 459.

[23] Y. Liang, H. Dong, D. Aurbach, Y. Yao, *Nat. Energy* 2020, *5*, 646–656.

[24] A. M. Abakumov, S. S. Fedotov, E. V. Antipov, J. .-M. Tarascon, *Nat. Commun.* 2020, *11*, 4976.

[25] S. Ferrari, M. Falco, A. B. Muñoz-García, M. Bonomo, S. Brutti, M. Pavone, C. Gerbaldi, *Adv. Energy Mater.* 2021, *11*, 2100785.

[26] S. Tang, W. Guo, Y. Fu, *Adv. Energy Mater.* 2021, *11*, 2000802.

[27] E. Manarin, F. Corsini, S. Trano, L. Fagiolari, J. Amici, C. Francia, S. Bodoardo, S. Turri, F. Bella, G. Griffini, *ACS Applied Polymer Materials* 2022, *4*, 5, 3855–3865.

[28] J. Wang, X. Liu, H. Jia, P. Apostol, X. Guo, F. Lucaccioni, X. Zhang, Q. Zhu, C. Morari, J. .-F. Gohy, A. Vlad, *ACS Energy Lett.* 2022, *7*, 2, 668–674.

[29] S. Trano, F. Corsini, G. Pascuzzi, E. Giove, L. Fagiolari, J. Amici, C. Francia, S. Turri, S. Bodoardo, G. Griffini, F. Bella, *ChemSusChem* 2022, *15*, e2022002.

[30] D. E. Fenton, J. M. Parker, P. V. Wright, *Polymer* 1973, *14*, 589.

[31] M. Armand, *Solid State Ionics* 1983, *9–10*, 745–754.

[32] W. H. Meyer, *Adv. Mater.* 1998, *10*, 439–448.

[33] J. Chai, Z. Liu, J. Zhang, J. Sun, Z. Tian, Y. Ji, K. Tang, X. Zhou, G. Cui, *ACS Appl. Mater. Interfaces* 2017, *9*, 17897.

[34] S. D. Tillmann, P. Isken, A. Lex-Balducci, *J. Power Sources* 2014, *271*, 239.

[35] S. D. Tillmann, P. Isken, A. Lex-Balducci, *J. Phys. Chem. C* 2015, *119*, 14873.

[36] F. Boujioui, F. Zhuge, H. Damerow, M. Wehbi, B. Améduri, J.-F. Gohy, *J. Mater. Chem. A* 2018, *6*, 8514.

[37] F. Boujioui, H. Damerow, F. Zhuge, J.-F. Gohy, *Macromol. Chem. Phys.* 2020, *221*, 1900556.

[38] J. Zhang, J. Zhao, L. Yue, Q. Wang, J. Chai, Z. Liu, X. Zhou, H. Li, Y. Guo, G. Cui, L. Chen, *Adv. Energy Mater.* 2015, *5*, 1501082.

[39] K. Kimura, M. Yajima, Y. Tominaga, *Electrochem. Commun.* 2016, *66*, 46.

[40] Y. Tominaga, V. Nanthana, D. Tohyama, *Polym. J.* 2012, *44*, 1155.

[41] T. Morioka, K. Nakano, Y. Tominaga, *Macromol. Rapid Commun.* 2017, *38*, 1600652.

[42] L. Meabe, T. V. Huynh, N. Lago, H. Sardon, C. Li, L. A. O'Dell, M. Armand, M. Forsyth, D. Mecerreyes, *Electrochim. Acta* 2018, *264*, 367.

Published in : ChemSusChem (2022), vol. 15, n°18, e202200913
DOI: doi.org/10.1002/cssc.202200913
Status : Postprint (Author's version)

[43] F. Ouhib, L. Meabe, A. Mahmoud, B. Grignard, J.-M. Thomassin, F. Boschini, H. Zhu, M. Forsyth, D. Mecerreyes, C. Detrembleur, *ACS Appl. Polym. Mater.* 2020, *2*, 922–931.

[44] M. Rayung, M. M. Aung, S. C. Azhar, L. C. Abdullah, M. S. Su'ait, A. Ahmad, N. A. Md Jamil, *Materials* 2020, *13*, 838.

[45] K. W. Chew, T. C. Ng, Z. H. How, *Int. J. Electrochem. Sci.* 2013, *8*, 6354– 6364.

[46] I. Osada, S. M. Hosseini, S. Jeong, S. Passerini, *ChemElectroChem* 2017, *4*, 463.

[47] Z. Lv, Y. Tang, S. Dong, Q. Zhou, G. Cui, *Chem. Eng. J.* 2022, *430*, 132659.

[48] M. S. M. Misenan, A. S. A. Khiarb, T. Eren, *Polym. Int.* 2022, *71*, 751–769.

[49] C. Carré, Y. Ecochard, S. Caillol, L. Avérous, *ChemSusChem* 2019, *12*, 3410–3430.

[50] N. Ren, Y. Song, C. Tao, B. Cong, Q. Cheng, Y. Huang, G. Xu, J. Bao, *J. Solid State Electrochem.* 2018, *22*, 1109–1121.

[51] S. Ibrahim, A. Ahmad, N. S. Mohamed, *Polymer* 2015, *7*, 747–759.

[52] S. R. Mustapa, M. M. Aung, M. Rayung, *Polymer* 2021, *13*, 132.

[53] M. Oshinowo, J. R. Runge, M. Piccini, F. Marken, A. Buchard, *J. Mater. Chem. A* 2022, *10*, 6796–6808.

[54] L. Zhang, H. Gao, G. Jin, S. Liu, J. Wu, H. Wu, Y. Yang, Q. Wang, S. Wang, *ChemNanoMat* 2022, e202200142.

[55] R. Alves, A. F. Marijuan, L. C. Arias, R. Gonçalves, M. M. Silva, F. J. D. Campo, C. M. Costa, S. L. Mendez, *ACS Appl. Mater. Interfaces* 2022, *14*, 15494–15503.

[56] C. W. Liew, S. Ramesh, *Cellulose* 2013, *20*, 3227–3237.

[57] A. S. A. Khiar, A. K. Arof, *Ionics* 2010, *16*, 123–129.

[58] L. Poussard, J. Mariage, B. Grignard, C. Detrembleur, C. Jérôme, C. Calberg, B. Heinrichs, J. De Winter, P. Gerbaux, J. M. Raquez, L. Bonnaud, P. Dubois, *Macromolecules* 2016, *49*, 2162–2171.

[59] X. Wei, D. F. Shriver, *Chem. Mater.* 1998, *10*, 2307–2308.

[60] S. S. Gupta, N. Solanki, A. T. M. Serajuddin, *AAPS PharmSciTech* 2016, *17*, 148–157.

[61] B. Scrosati, C. A. Vincent, *MRS Bull.* 2000, *25*, 28–30.

[62] R. C. Agrawal, G. P. Pandey, *J. Phys. D.* 2008, *4*, 3715–3725.

[63] P. L. Kuo, W. J. Liang, T. Y. Chen, *Polymer* 2003, *44*, 2957–2964.

[64] J. Mindemark, B. Sun, E. Törmä, D. Brandell, *J. Power Sources* 2015, *298*, 166–170.

[65] L. Meabe, N. Lago, L. Rubatat, C. Li, A. J. Müller, H. Sardon, M. Armand, D. Mecerreyes, *Electrochim. Acta* 2017, *237*, 259–266.

[66] J. R. MacCallum, C. A. Vincent Eds., *Polymer Electrolyte Reviews 1*, Elsevier, London, 1987, 23.

Published in : ChemSusChem (2022), vol. 15, n°18, e202200913
DOI: doi.org/10.1002/cssc.202200913
Status : Postprint (Author's version)

[67] N. K. Karan, D. K. Pradhan, R. Thomas, B. Natesan, R. S. Katiyar, *Solid State Ionics* 2008, *179*, 689–696.

[68] T. Miyamoto, K. J. Shibayama, *J. Appl. Phys.* 1973, *44*, 5372.

[69] J. Xi, X. Qiu, M. Cui, X. Tang, W. Zhu, L. Chen, *J. Power Sources* 2006, *156*, 581.

[70] Y. R. Zhao, Z. Huang, S. J. Chen, B. Chen, J. Yang, Q. Zhang, F. Ding, Y. H. Chen, X. X. Xu, *Solid State Ionics* 2016, *295*, 65–71.

[71] J. Evans, C. A. Vincent, P. G. Bruce, *Polymer* 1987, *28*, 2324.

[72] P. G. Bruce, C. A. Vincent, *J. Electroanal. Chem. Interfacial Electrochem.* 1987, *225*, 1–17.

[73] S. Han, *Sci. Rep.* 2019, *9*, 5555.

[74] M. Rosso, C. Brissot, A. Teyssot, M. Dollé, L. Sannier, J. .-M. Tarascon, R. Bouchet, S. Lascaud, *Electrochim. Acta* 2006, *51*, 5334–5340.

[75] R. Bouchet, S. Maria, R. Meziane, A. Aboulaich, L. Lienafa, J. P. Bonnet, T. N. T. Phan, D. Bertin, D. Gigmes, D. Devaux, R. Denoyel, M. Armand, *Nat. Mater.* 2013, *12*, 452–457.

[76] R. Meziane, J. P. Bonnet, M. Courty, K. Djellab, M. Armand, *Electrochim. Acta* 2011, *570*, 14–19.

[77] Z. Y. Cui, Y. Y. Xu, L. P. Zhu, J. Y. Wang, Z. Y. Xi, B. K. Zhu, *J. Membr. Sci.* 2008, *325*, 957.

[78] L. L. Liu, Z. H. Li, Q. L. Xia, Q. Z. Xiao, G. T. Lei, X. D. Zhou, *Ionics* 2012, *18*, 275–281.

[79] R. Khurana, J. L. Schaefer, L. A. Archer, G. W. Coates, *J. Am. Chem. Soc.* 2014, *136*, 20, 7395–7402.

[80] K. N. Wood, G. Teeter, *ACS Appl. Energ. Mater.* 2018, *1*, 4493–4504.

[81] P. Shi, L. Zhang, H. Xiang, X. Liang, Y. Sun, W. Xu, *ACS Appl. Mater. Interfaces* 2018, *10*, 22201–22209.

[82] S. Leroy, H. Martinez, R. Dedryvere, D. Lemordant, D. Gonbeau, *Appl. Surf. Sci.* 2007, *253*, 4895–4905.

[83] R. Grissa, V. Fernandez, N. Fairley, J. Hamon, N. Stephant, J. Rolland, R. Bouchet, M. Lecuyer, M. Deschamps, D. Guyomard, *ACS Appl. Energ. Mater.* 2018, *1*, 5694–5702.

[84] S. Panchireddy, J.-M. Thomassin, B. Grignard, C. Damblon, A. Tatton, C. Jerome, C. Detrembleur, *Polym. Chem.* 2017, *8*, 5897–5909.

[85] S. Gennen, M. Alves, R. Méreau, T. Tassaing, B. Gilbert, C. Detrembleur, C. Jerome, B. Grignard, *ChemSusChem* 2015, *8*, 1845–1849.

[86] M. Alves, B. Grignard, S. Gennen, R. Mereau, C. Detrembleur, C. Jérôme, T. Tassaing, *Catal. Sci. Technol.* 2015, *5*, 4636–4643.

[87] M. Alves, B. Grignard, S. Gennen, C. Detrembleur, C. Jerome, T. Tassaing, *RSC Adv.* 2015, *5*, 53629–53636.

[88] G. Karmakar, P. Ghosh, *ACS Sustainable Chem. Eng.* 2016, *4*, 775–781.

Published in : ChemSusChem (2022), vol. 15, n°18, e202200913
DOI: doi.org/10.1002/cssc.202200913
Status : Postprint (Author's version)

[89] A. Ghosal, O. U. Rahman, S. Ahmad, *Ind. Eng. Chem. Res.* 2015, *54*, 12770–12787.

[90] M. Sacristán, J. C. Ronda, M. Galià, V. Cádiz, *Biomacromolecules* 2009, *10*, 2678–2685.

[91] C. Zhang, Y. Xia, R. Chen, S. Huh, P. A. Johnston, M. R. Kessler, *Green Chem.* 2013, *15*, 1477–1484.